ACS APPLIED MATERIALS & INTERFACES

Research Article

www.acsami.org

Low-Cost Label-Free Electrical Detection of Artificial DNA Nanostructures Using Solution-Processed Oxide Thin-Film Transistors

Si Joon Kim,[†] Joohye Jung,[†] Keun Woo Lee,[†,‡] Doo Hyun Yoon,[†] Tae Soo Jung,[†] Sreekantha Reddy Dugasani,[‡] Sung Ha Park,*[,‡] and Hyun Jae Kim*[,†]

[†]School of Electrical and Electronic Engineering, Yonsei University, 50 Yonsei-ro, Seodaemun-gu, Seoul 120-749, Republic of Korea

[‡]Department of Physics and SKKU Advanced Institute of Nanotechnology (SAINT), Sungkyunkwan University, Suwon, Gyeonggi-do 440-746, Republic of Korea

Supporting Information

ABSTRACT: A high-sensitivity, label-free method for detecting deoxyribonucleic acid (DNA) using solution-processed oxide thin-film transistors (TFTs) was developed. Double-crossover (DX) DNA nanostructures with different concentrations of divalent Cu ion (Cu^{2+}) were immobilized on an In−Ga−Zn−O (IGZO) back-channel surface, which changed the electrical performance of the IGZO TFTs. The detection mechanism of the IGZO TFT-based DNA biosensor is attributed to electron trapping and electrostatic interactions caused by negatively charged phosphate groups on the DNA backbone. Furthermore, Cu^{2+} in DX DNA nanostructures generates a current path when a gate bias is applied. The direct effect on the electrical response implies that solution-processed IGZO TFTs could be used to realize low-cost and high-sensitivity DNA biosensors.

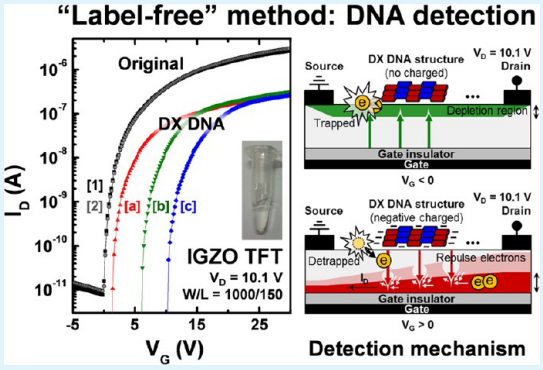

KEYWORDS: *oxide semiconductor, thin-film transistors, solution process, DNA nanostructure, biosensors*

1. INTRODUCTION

To satisfy human's desires for good health and longevity, medical science and biotechnology are making great progress. After many experiments and much research, it has been virtually identified that every human illness is associated with a hereditary component.[1,2] In this regard, it is necessary to understand and analyze genetic information. Specifically, deoxyribonucleic acid (DNA) detection technology, one of the most powerful methods for gene investigation, has become increasingly important for unraveling genetic diseases and for improving medical diagnosis and treatment.[3−13]

Until recently, fluorescence techniques have been mainly used for detecting DNA.[3−5] Unfortunately, this traditional method of DNA detection is both time-consuming and costly, as it requires attaching fluorescent molecules to the target DNA and scanning the fabricated DNA chip with an optical system. Therefore, fluorescence techniques are unsuitable for direct and rapid medical diagnosis and low-cost portable DNA-sensing systems.

For quick and easy DNA detection, various label-free field effect transistor (FET) systems have been developed.[6−13] Compared with other label-free techniques, general FETs are ideal for use in DNA biosensors because the fabrication of small-sized and high-density FET arrays is mature technology, and this process can be transferred directly to DNA sensing systems. Moreover, FET-based DNA biosensors show high sensitivity and direct transduction.[11−13] In particular, thin-film transistors (TFTs), which are similar to other FETs in terms of device operation and structure, have great advantages: they can be adapted to various insulating substrates (glass or flexible ones) and involve a simple process without additional doping (no p-n junctions). This implies that TFT-based DNA biosensors have a broad range of applications and potentially lower manufacturing costs. In this regard, label-free DNA detection methods using TFTs based on organic semiconductor materials and nanomaterials such as carbon nanotubes, graphene, nanowires, and nanoparticles have been studied intensively.[6−10] However, organic TFTs have reliability and reproducibility problems such as process-dependent performance variation, and the fabrication of nanomaterials is complicated and expensive.[13] Therefore, this paper investigated the applicability of oxide semiconductor materials as a biosensitive layer for detecting immobilized DNA.

Oxide semiconductor materials represented by In−Ga−Zn−O (IGZO) have been broadly reported for use in TFTs as a pixel component for flat panel and next-generation displays.[14−18] Compared with the other materials mentioned above, oxide semiconductor materials have many advantages, including superior electrical properties, high reliability, and easy reprodu-

Received: July 16, 2013
Accepted: September 27, 2013
Published: September 27, 2013

cibility.[14−18] Previously, we described DNA sensing capability using IGZO TFTs for the first time.[11] However, there is still insufficient knowledge of the DNA detection mechanism and the ability to sense different DNA molecules.

Here, we fabricated and investigated solution-processed IGZO TFTs to validate their DNA sensing ability and detection mechanism. For an in-depth analysis, we used artificially designed double-crossover (DX) DNA nanostructures with various concentrations of divalent Cu ion (Cu^{2+}) and studied the electrical responses of the IGZO TFTs with and without DX DNA immobilization.

2. EXPERIMENTAL PROCEDURE

A 0.3 M IGZO solution was synthesized using indium nitrate hydrate [$In(NO_3)_3{\cdot}xH_2O$], gallium nitrate hydrate [$Ga(NO_3)_3{\cdot}xH_2O$], zinc acetate dihydrate [$Zn(CH_3COO)_2{\cdot}2H_2O$] in 2-methoxyethanol (2ME) solvent. As stabilizers, monoethanolamine (MEA) and acetic acid (CH_3COOH) were dropped to ameliorate the solubility of the precursors and make a homogeneous IGZO solution, respectively. The mixture was stirred for 1 h at 60 °C, filtered through a 0.2 μm microfilter, and then aged for at least 24 h in ambient air.

To prepare of TFT devices, the bottom-gate and top-contact structure was used in the process depicted in Figure 1. First, 200-nm-thick MoW was deposited on a SiO_2/glass substrate by sputtering and then patterned as a gate electrode. The blocking layer of SiO_2 protects the TFT from impurities originating in the glass during the subsequent processes. Then, 200 nm thick SiN_x was deposited by plasma-enhanced chemical vapor deposition as a gate insulator. The synthesized IGZO solution was spin coated at a speed of 3000 rpm for 30 s in ambient nitrogen. The IGZO thin-film was preannealed at 300 °C for 5 min to remove the 2ME solvent and annealed at 500 °C for 2 h on a hot plate to develop an active layer. Finally, 200 nm thick Mo source and drain electrodes were deposited on this IGZO thin-film via a shadow mask by sputtering. The channel length (L) and width (W) of IGZO TFTs were 150 and 1000 μm, respectively.

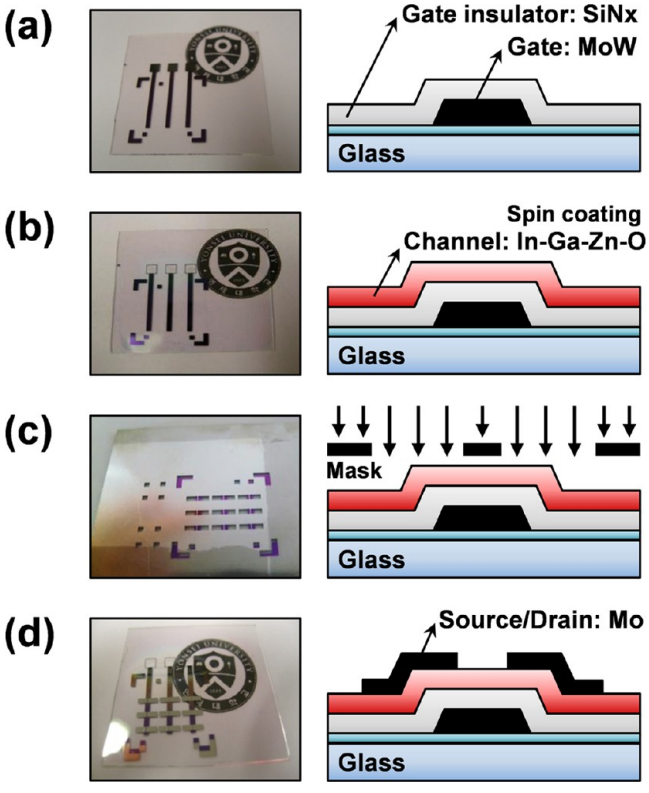

Figure 1. Schematic and optical image of the procedure used to fabricate solution-processed IGZO TFT devices. (a) MoW as a gate electrode and SiN_x as a gate insulator were used. (b) Solution-processed IGZO thin-film was used as an active layer. (c) Mo was deposited via a shadow mask and (d) employed for source and drain electrodes.

Two DX tiles were used to construct a two-dimensional (2D) DNA nanostructure, which was fabricated using the conventional free solution annealing process.[19] Complexes were formed by mixing a stoichiometric quantity of each strand in physiological 1 × TAE/Mg^{2+} buffer (Tris-acetate-ethylenediaminetetraacetic acid [EDTA], 40 mM Tris-base, 1 mM EDTA [pH 8.0], and 12.5 mM $Mg(acetate)_2$) to produce the DX structure. To facilitate hybridization, the complexes were cooled slowly from 95 to 25 °C by placing the microtubes in 2 L of boiled water in a Styrofoam box for at least 24 h. The final concentration of the DX DNA lattices was 200 nM. After annealing DX lattices in a test tube, the appropriate amount of 1 M concentration of Cu^{2+} solution [$Cu(NO_3)$]$_2$ was added and then incubated at room temperature for 24 h. These prepared DX DNA solutions with different Cu^{2+} concentrations are shown in the insets in Figure 3a, Figure 5d, and Figure 5e. For atomic force microscopy (AFM), the experiment was performed in fluid tapping mode under 1 × TAE/Mg^{2+} buffer. Prepared DNA-covered mica sheet was attached onto the metal puck using instant glue and 5 μL of DX solution, 30 μL of 1 × TAE/Mg^{2+} buffer was dropped onto the mica and 10 μL of 1 × TAE/Mg^{2+} buffer was mounted onto the AFM tip (A NP-S oxide-sharpened silicon nitride tip).

Physical and chemical immobilization techniques have been employed to immobilize biomolecules on oxide based materials.[11,12,20−22] Among them, physical immobilization using methods such as adsorption, entrapment, confinement, and encapsulation has been predominantly used because of the high isoelectric point of oxide-based materials.[22] In this work, the artificially designed DX DNA solution was dropped onto the exposed IGZO back-channel surface (sensing area) using micro pipet (0.5 μL) and air-dried at least 300 min. Then, DX DNA nanostructure was immobilized physically on the exposed IGZO channel.

3. RESULTS AND DISCUSSION

Figure 2a shows a cross-sectional high-resolution transmission electron microscopy (HR-TEM) image of the fabricated IGZO

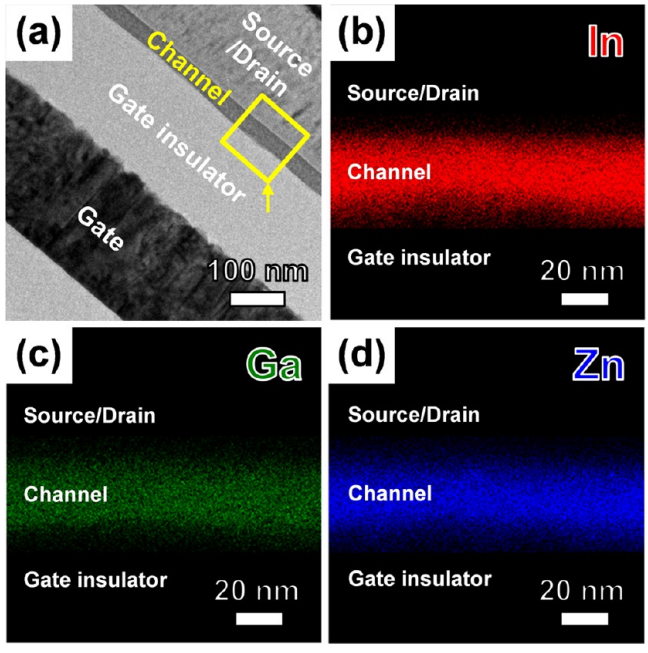

Figure 2. (a) Cross-sectional HR-TEM images of the IGZO TFT structure and compositional mapping for (b) In, (c) Ga, and (d) Zn obtained from EDS analysis.

TFT device. From HR-TEM image, we verified the validity of the experimental scheme and confirmed the thickness of each layer, including the IGZO channel layer (about 30 nm). The selected area electron-diffraction (SAED) patterns of the IGZO thin-film revealed that this channel layer has a nanocrystalline phase in an amorphous matrix (data not shown). This is consistent with the X-ray diffraction (XRD) pattern of the IGZO thin-film (see the Supporting Information, Figure S2b).

To investigate the homogeneity of the IGZO thin-film (marked by the arrow in Figure 2a), the compositional mapping of three metallic constituents (In, Figure 2b; Ga, Figure 2c; and Zn, Figure 2d) was observed using energy-dispersive X-ray spectroscopy (EDS) analysis while operating in scanning TEM (STEM) mode. A uniform distribution was observed (i.e., no elemental segregation or phase separation), and then this result clearly indicated that the synthesized IGZO solution and the fabricated IGZO thin-film were homogeneous, as expected.

The superior electrical properties of IGZO TFTs arise from the conduction band minimum composed of the spatially spread ns orbitals of In heavy metal with an isotropic shape and the direct overlap between them (n is the principal quantum number). Because the molar ratio of the synthesized IGZO solution was fixed in this work (In:Ga:Zn = 5:1:2), the In metallic constituent comprised a relatively large percentage of the overall IGZO thin-film (In:Ga:Zn = 24.85:5.97:12.84 atomic percentage obtained from EDS analysis). Consequently, the sensitivity of the IGZO TFT-based DNA biosensor, in which the electrical responses are contingent upon DNA immobilization, was improved significantly compared with other types of TFTs, for instance, organic TFTs.[23−25]

Because the IGZO TFT is susceptible to water molecules,[26−28] the use of water-based DNA solutions is limited. The dry-wet method (DWM)[11,12,29,30] was used instead of a water-based solvent. A prepared DX DNA solution was placed into a fume hood for about 24 h to evaporate all water molecules, and then dried samples were reconstituted in a nonaqueous solvent; ethanol was used in this research. When the polar solvent, ethanol, was dropped on the exposed IGZO back-channel surface, the IGZO TFT exhibited negative threshold voltage (V_{th}) and turn-on voltage (V_{on}) shifts and a subthreshold swing (SS) degradation without accompanying degradation of field effect mobility (μ_{FET}).[28] This degradation recovered gradually to the initial state without any treatment, such as annealing process, due to the rapid evaporation of the ethanol molecules.[28] Consequently, an ethanol-based DNA solution is appropriate for restoring and delivering DX DNA nanostructures to the exposed IGZO channel.

Generally, the electrical performance of IGZO TFT devices is analyzed based on the drain current (I_D)-gate voltage (V_G) transfer characteristics when the drain voltage (V_D) is fixed (at 10.1 V in this work). Parameters such as the μ_{FET}, V_{th}, SS, and maximum trapped charge density (N_{max}) were extracted from the transfer characteristics using the following equation:

$$\mu_{FET} = \left(\frac{2}{C_i}\right)\left(\frac{L}{W}\right)(G_{max})^2,\ V_{th} = V_G - \frac{\sqrt{I_D}}{G_{max}}$$

$$\text{when } G = \frac{\partial\sqrt{I_D}}{\partial V_G}(V_D > V_G - V_{th}, \text{ saturation region})$$

$$SS = \frac{dV_G}{d\log(I_D)}(V_G < V_{th}, \text{ subthreshold region})$$

$$N_{max} = \left(\frac{SS\log(e)}{kT/q} - 1\right)\frac{C_i}{q}$$

where C_i is the gate capacitance per unit area, G_{max} is the maximum gradient (G), k is the Boltzmann constant, T is the room temperature, and q is the elementary charge. In addition, the on-current (I_{on}) is the maximum I_D, the off-current (I_{off}) is the minimum I_D, and the V_{on} is the V_G when I_D starts to increase abruptly.

Figure 3a shows the transfer characteristics of IGZO TFT with and without DX DNA immobilization. The measuring device

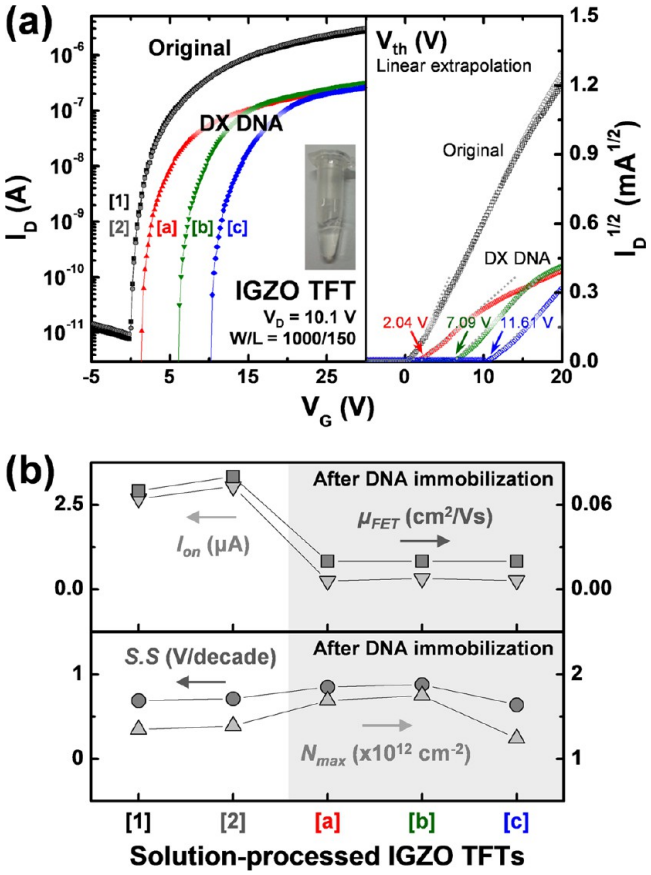

Figure 3. (a) Transfer characteristics of the IGZO TFT before and after DX DNA immobilization; (b) variations in μ_{FET}, I_{on}, SS, and N_{max} when V_G is swept repeatedly.

behaves like a typical n-type transistor, which means that the dominant carrier in IGZO TFT is electrons. When the applied V_G exceeds V_{on}, electrons are injected from the source electrode to the drain electrode through a relatively low-resistance region of IGZO thin-film (i.e., electron accumulation region induced by the positive gate bias exists at the interface between IGZO active layer and SiN_x gate insulator). This electron transport is related to the flow of I_D in the opposite direction from the drain electrode to the source electrode, and the magnitude of the I_D flow is determined primarily by the charge density of the accumulation region and the magnitude of V_D.

Before DX DNA immobilization, we observed no variation in the transfer characteristics when V_G was repeatedly swept from −5 to +30 V ([1] and [2] in Figure 3). This result is related to the reliability of the IGZO TFT devices. However, significant decreases in μ_{FET} and I_{on} of the IGZO TFT were observed after

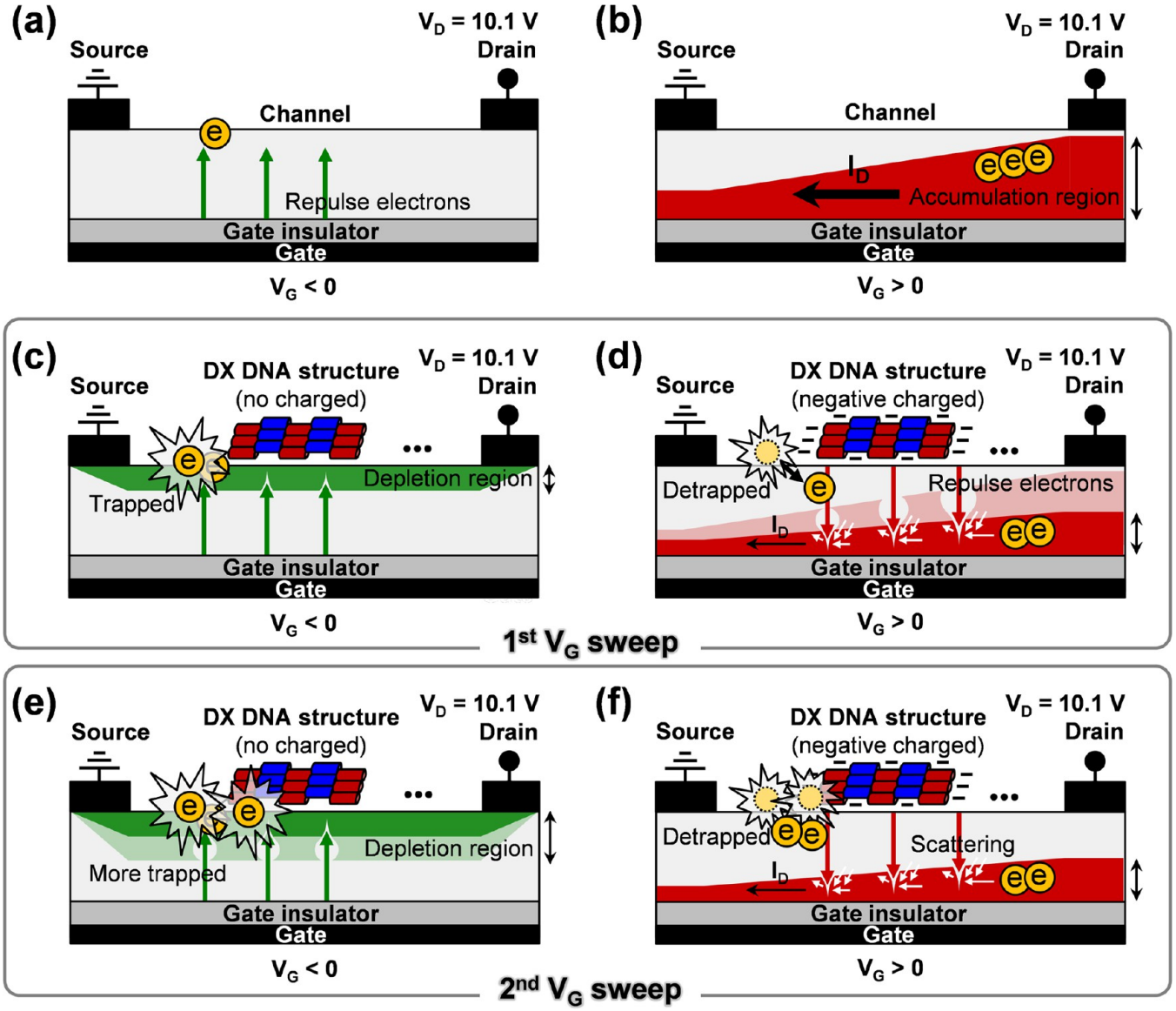

Figure 4. Schematic of the DNA detection mechanism: (a, b) before and after DX DNA immobilization during the (c, d) first and (e, f) second sweep of V_G from −5 to +30 V with V_D fixed at 10.1 V, respectively.

DX DNA immobilization as shown in Figure 3b. Moreover, we observed progressive shifts of V_{th} and V_{on} in the positive direction without an accompanying degradation in *S.S* and N_{max} when V_G was swept three times repeatedly ([a], [b], and [c] in Figure 3).

Figure 4 shows the DX DNA detection mechanism according to the V_G sweep. When a negative gate bias was applied to an IGZO TFT containing immobilized DX DNA, the repulsed electrons were trapped at the DX DNA nanostructure, and a depletion region formed near the IGZO channel surface, as shown in Figure 4c. As the gate bias changed from negative to positive, it took some time to detrap these trapped electrons from the DX DNA shifting V_{th} and V_{on} in a positive direction. Moreover, the DX DNA nanostructure, which has negatively charged phosphate groups on the backbone, repulsed electrons, including the detrapped electrons, from the IGZO channel surface to the SiN_x gate insulator. Consequently, the electron scattering in the accumulation region increased as shown in Figure 4d. The electrostatic interactions so generated caused significant decreases in μ_{FET} and I_{on}. Given that we fixed V_D at 10.1 V in this work, the magnitude of the reduction in I_D was considered to be the only factor related to the charge density of the accumulation region, and this corroborated the explanation of the DX DNA detection mechanism. During the second V_G sweep, these phenomena were repeated as shown in Figure 4e and Figure 4f. Because the concentration of the immobilized DX DNA nanostructure was fixed, no more degradation of μ_{FET} and I_{on} was observed as shown in Figure 3b. Although the electrons were trapped further when a negative gate bias was again applied, with strengthened positive V_{th} and V_{on} shifts as shown in Figure 3a, these shifts of the transfer characteristics were saturated eventually.

Figure 5a–c shows AFM images of DX DNA lattices with Cu^{2+} concentrations of 0, 5, and 10 mM, respectively. To keep the structural stability of the metal ion-coordinated DNA lattice as similar as possible to that of the DNA lattice without metal ions, the experimental procedure involved adding Cu^{2+} to the DNA buffer solution after annealing. On the basis of AFM, the surface morphologies of the DNA nanostructures at the two different Cu^{2+} concentrations did not differ from that of the DNA lattice without Cu^{2+}.

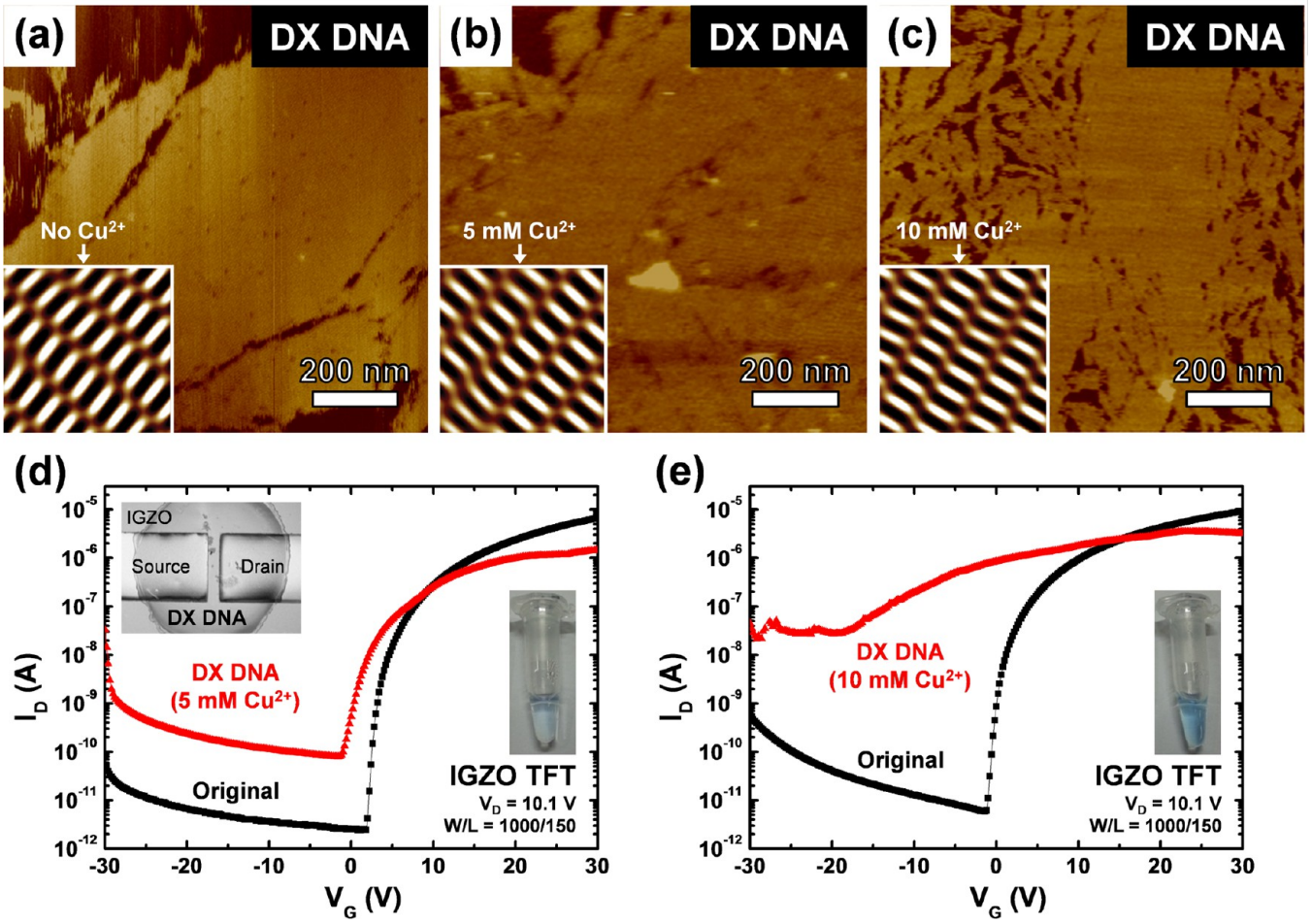

Figure 5. AFM images of the DX DNA lattice with (a) 0 mM Cu^{2+}, (b) 5 mM Cu^{2+}, and (c) 10 mM Cu^{2+}. Insets in the bottom left corner are noise-filtered 2D spectrum by Fourier transform showing the periodicity of the lattice (scan size, 50 × 50 nm^2). Transfer characteristics of the IGZO TFTs before and after DX DNA immobilization with (d) 5 mM Cu^{2+} and (e) 10 mM Cu^{2+}.

The transfer characteristics of the IGZO TFTs before and after DX DNA immobilization are shown with 5 mM Cu^{2+} (Figure 5d) and 10 mM Cu^{2+} (Figure 5e). In both cases, I_{on} decreased, which was analogous to the detection mechanism of the DX DNA lattice without Cu^{2+}. However, there were some differences in the magnitude of the reduction in I_{on} and the variation in I_{off}. Consequently, we need an additional mechanism to explain the detection of the Cu^{2+}-modified DX DNA nanostructure. When a negative gate bias was applied, the current path between the source and drain electrodes was generated via a conducting material, Cu^{2+}, and then I_{off} increased. Although a decrease in I_{on} was observed because of the negatively charged phosphate groups on the DNA backbone, this reduction in I_{on} was compensated for by the current path that resulted from Cu^{2+}. Therefore, it is possible to control the conductivity of the DX DNA nanostructure, and the sensitivity of IGZO TFT-based DNA biosensors is improved using these conductivity-controllable DNA nanostructures. The variation in the electrical parameters is summarized in Table 1 and the detection mechanism of the DX DNA nanostructure with Cu^{2+} modification is shown in Figure 6 (see the Supporting Information, Figure S1).

To further investigate the method of detecting DX DNA nanostructures, we examined the optical transmittance and XRD patterns; no significant variation was exhibited (see the Supporting Infroamtion, Figure S2). Furthermore, we examined

Table 1. Comparison of the Electrical Parameters of Solution-Processed IGZO TFTs after DX DNA Immobilization (DX Lattice with Different Cu^{2+} Concentrations)

	DX lattice with 5 mM Cu^{2+}		DX lattice with 10 mM Cu^{2+}	
params	before	after	before	after
μ_{FET} ($cm^2\ V^{-1}\ s^{-1}$)	0.12	0.06	0.14	0.04
I_{on} (μA)	6.63	1.45	9.24	3.47
I_{off} (pA)	2.39	78.80	5.89	2.13×10^4
SS ($V\ dec^{-1}$)	0.63	1.38	0.68	5.4
V_{th} (V)	5.62	2.45	1.59	−16.68
V_{on} (V)	1.20	−1.60	−1.40	−19.00

AFM images of IGZO thin-films as prepared before DNA immobilization, with 5-helix ribbon (5HR) DNA nanostructures, and with DX DNA nanostructures (see the Supporting Information, Figures S3 and S4). The 5HR DNA nanostructure is relatively thick (i.e., microscale) compared with the DX DNA nanostructure and thus is clearly distinguishable in the AFM images. By contrast, the nanoscale thickness of the DX DNA nanostructure cannot be detected directly using AFM due to the relatively high degree of roughness of the IGZO thin-film, which has about 1.2 nm root-mean-square roughness. Therefore, solution-processed IGZO TFTs, a label-free method, are

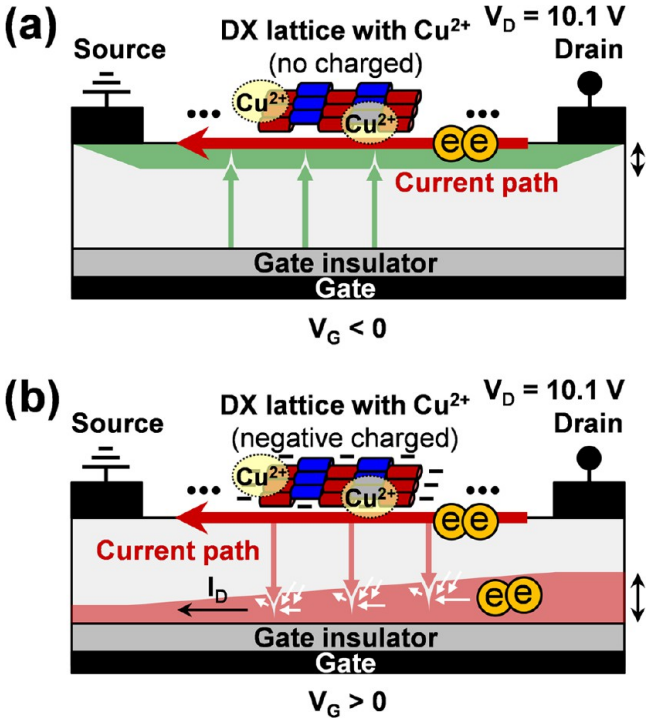

Figure 6. Schematic of the DNA detection mechanism for DX DNA immobilization after adding Cu^{2+} and applying (a) negative and (b) positive gate biases.

commensurate with low-cost and high-sensitivity DNA biosensors.

4. CONCLUSION

In summary, solution-processed IGZO TFTs were investigated for application in DX DNA nanostructure sensing. DX DNA nanostructures with different Cu^{2+} concentrations were immobilized physically on the surface of the IGZO channel layers and directly affected the electrical response of the IGZO TFTs. The detection mechanism of the IGZO TFT-based DNA biosensor is attributed to electron trapping and electrostatic interactions caused by negatively charged phosphate groups on the DNA backbone. Furthermore, Cu^{2+} in DNA nanostructures generates a current path when a gate bias is applied. Therefore, solution-processed IGZO TFTs, a label-free method for DNA detection with high sensitivity, enable the realization of direct and rapid medical diagnosis and low-cost portable DNA sensing systems.

■ ASSOCIATED CONTENT

Ⓢ Supporting Information

Additional figures (PDF). This material is available free of charge via the Internet at http://pubs.acs.org.

■ AUTHOR INFORMATION

Corresponding Authors

*E-mail: sunghapark@skku.edu.
*E-mail: hjk3@yonsei.ac.kr.

Notes

The authors declare no competing financial interest.

■ ACKNOWLEDGMENTS

This work was supported by the National Research Foundation of Korea (NRF) grant funded by the Korean Ministry of Education, Science and Technology (MEST) (2011-0028819).

■ REFERENCES

(1) Collins, F. S. *N. Engl. J. Med.* **1999**, *341*, 28−37.
(2) Collins, F. S.; McKusick, V. A. *JAMA* **2001**, *285*, 540−544.
(3) Singh, N. P.; Mccoy, M. T.; Tice, R. R.; Schneider, E. L. *Exp. Cell. Res.* **1988**, *175*, 184−191.
(4) DeRisi, J. L.; Iyer, V. R.; Brown, P. O. *Science* **1997**, *278*, 680−686.
(5) Wittwer, C. T.; Herrmann, M. G.; Moss, A. A.; Rasmussen, R. P. *BioTechniques* **1997**, *22*, 130−138.
(6) Zhang, Q.; Subramanian, V. *Biosens. Bioelectron.* **2007**, *22*, 3182−3187.
(7) Lai, S.; Demelas, M.; Casula, G.; Cosseddu, P.; Barbaro, M.; Bonfiglio. *Adv. Mater.* **2013**, *25*, 103−107.
(8) Sorgenfrei, S.; Chiu, C.-Y.; Gonzalez, R. L., Jr.; Yu, Y.-J.; Kim, P.; Nuckolls, C.; Shepard, K. L. *Nat. Nanotechnol.* **2011**, *6*, 126−132.
(9) Yin, Z.; He, Q.; Huang, X.; Zhang, J.; Wu, S.; Chen, P.; Lu, G.; Chen, P.; Zhang, Q.; Yan, Q.; Zhang, H. *Nanoscale* **2012**, *4*, 293−297.
(10) Vu, X. T.; GhoshMoulick, R.; Eschermann, J. F.; Stockmann, R.; Offenhausser, A.; Ingebrandt, S. *Sens. Actuators, B* **2010**, *144*, 354−360.
(11) Kim, S. J.; Kim, B.; Jung, J.; Yoon, D. H.; Lee, J.; Park, S. H.; Kim, H. J. *Appl. Phys. Lett.* **2012**, *100*, 103702−1−103702−4.
(12) Jung, J.; Kim, S. J.; Yoon, D. H.; Kim, B.; Park, S. H.; Kim, H. J. *ACS Appl. Mater. Interfaces* **2013**, *5*, 98−102.
(13) Yan, F.; Tang, H. *Expert Rev. Mol. Diagn.* **2010**, *10*, 547−549.
(14) Nomura, K.; Ohta, H.; Ueda, K.; Kamiya, T.; Hirano, M.; Hosono, H. *Science* **2003**, *300*, 1269−1272.
(15) Nomura, K.; Ohta, H.; Takagi, A.; Kamiya, T.; Hirano, M.; Hosono, H. *Nature* **2004**, *432*, 488−492.
(16) Kim, S. J.; Kim, D. L.; Kim, D. N.; Kim, H. J. *J. Inf. Disp.* **2010**, *11*, 165−168.
(17) Kim, S. J.; Yoon, D. H.; Rim, Y. S.; Kim, H. J. *Electrochem. Solid-State Lett.* **2011**, *14*, E35−E37.
(18) Fortunato, E.; Barquinha, P.; Martins, R. *Adv. Mater.* **2012**, *24*, 2945−2986.
(19) Shin, J.; Kim, J.; Amin, R.; Kim, S.; Kwon, Y. H.; Park, S. H. *ACS Nano* **2011**, *5*, 5175−5179.
(20) Reyes, P. I.; Ku, C.-J.; Duan, Z.; Lu, Y.; Solanki, A.; Lee, K.-B. *Appl. Phys. Lett.* **2011**, *98*, 173702−1−173702−3.
(21) Kumar, N.; Dorfman, A.; Hahm, J. *Nanotechnology* **2006**, *17*, 2875−2881.
(22) Arya, S. K.; Saha, S.; Ramirez-Vick, J. E.; Gupta, V.; Bhansali, S.; Singh, S. P. *Anal. Chim. Acta* **2012**, *737*, 1−21.
(23) Yan, F.; Mok, S. M.; Yu, J.; Chan, H. L. W.; Yang, M. *Biosens. Bioelectron.* **2009**, *24*, 1241−1245.
(24) Kim, J.-M.; Jha, S. K.; Chand, R.; Lee, D.-H.; Kim, Y.-S. *Biosens. Bioelectron.* **2011**, *26*, 2264−2269.
(25) Liu, N.; Hu, Y.; Zhang, J.; Cao, J.; Liu, Y.; Wang, J. *Org. Electron.* **2012**, *13*, 2781−2785.
(26) Park, J.-S.; Jeong, J. K.; Chung, H.-J.; Mo, Y.-G.; Kim, H. D. *Appl. Phys. Lett.* **2008**, *92*, 072104−1−072104−3.
(27) Chung, W.-F.; Chang, T.-C.; Li, H.-W.; Chen, C.-W.; Chen, Y.-C.; Chen, S.-C.; Tseng, T.-Y.; Tai, Y.-H. *Electrochem. Solid-State Lett.* **2011**, *14*, H114−H116.
(28) Kim, S. J.; Jung, J.; Yoon, D. H.; Kim, H. J. *J. Phys. D: Appl. Phys.* **2013**, *46*, 035102−1−035102−5.
(29) Lee, K. W.; Kim, K. M.; Lee, J.; Amin, R.; Kim, B.; Park, S. K.; Lee, S. K.; Park, S. H.; Kim, H. J. *Nanotechnology* **2011**, *22*, 375202−1−375202−6.
(30) Lee, J.; Amin, R.; Kim, B.; Ahn, S. J.; Lee, K. W.; Kim, H. J.; Park, S. H. *Soft Matter* **2012**, *8*, 619−622.